

EFFECT OF ENERGY DENSITY AND HOT ISOSTATIC PRESSING ON MICROSTRUCTURE AND POROSITY IN LASER POWDER BED FUSION-PROCESSED TIGALAY ALLOY

Tomáš ČEGAN, Kateřina SKOTNICOVÁ, Jan JUŘICA, Lukáš HORSAK

Faculty of Materials Science and Technology, VSB – Technical University of Ostrava, Ostrava, Czech Republic, EU, tomas.cegan@vsb.cz

https://doi.org/10.37904/metal.2025.5090

Abstract

Among titanium-based alloys, Ti-6Al-4V is the most extensively utilized material for structural applications due to its exceptional strength-to-weight ratio, outstanding corrosion resistance, and excellent biocompatibility. It has been widely processed via laser powder bed fusion (L-PBF), a leading additive manufacturing technique that allows for the fabrication of near-net-shape components, offering substantial cost and material savings. The processing parameters employed in L-PBF critically influence the resulting microstructure, defect formation, and mechanical performance of the alloy. This study focuses on the microstructural features and relative density of Ti-6Al-4V components manufactured under varying energy densities. The findings reveal that defect generation is highly sensitive to the applied energy density, with a marked effect on key mechanical properties, especially ductility. Furthermore, the results indicate that higher laser power can mitigate the sensitivity of other processing variables, enabling the production of high-quality parts at increased scanning speeds and reduced build times. A detailed analysis of individual process parameters is presented, along with an evaluation of the effects of hot isostatic pressing (HIP) and post-process heat treatments on the evolution of the microstructure and the enhancement of mechanical properties.

Keywords: Powder bed fusion, Ti6Al4V alloy, energy density, heat treatment, hot isostatic pressing

1. INTRODUCTION

Metal-based additive manufacturing (AM) enables manufacturing of metal parts with a high degree of geometric complexity and promises to significantly reduce cost, time, and energy consumption of production [1]. For example, the "buy-to-fly" ratio (the mass ratio between the raw material used to produce a component and the mass of the component) is 12-25:1 for aircraft titanium products made by traditional manufacturing methods, while it drops to 3-12:1 for a typical titanium component manufactured by AM processes [2-4]. Currently, probably the most widely used additive technology for metal preparation is laser beam powder bed fusion (L-PBF). L-PBF is a technology where the powder bed, deposited on the build platform (BP) by a recoater roller or blade, is scanned and melted through a laser beam characterized by a laser power P [W], and generated by one of the following energy sources: Yb:YAG fiber, Nd:YAG, CO2 laser, infrared, etc. [5]. During the L-PBF process, the laser beam transmits enough energy to melt the entire layer depth and a portion of the previously solidified layer, guaranteeing the adhesion between them [5]. The molten pool (MP) depth is key to obtaining this adhesion and the absence of defects. However, even with the use of appropriate L-PBF parameters, internal defects often occur in the products. L-PBF is a relatively complex process in terms of solidification, which is very fast and dynamic, but is influenced by many variables and physical processes: the quality of the input powder, evaporation during melting, convection in the melt, or denudation [1-6]. In terms of solidification, selective melting and solidification occur in a large number of places in the volume of the prepared material and at each place of the powder bed the local conditions may be slightly different, which can cause defects and reduce the reproducibility of the process [1,4,5]. Another problem is usually high internal stress in the products caused by rapid solidification during printing and anisotropy of the microstructure. For the above reasons, additional heat treatment of products is usually applied [4,5,7-10]. Ti6Al4V alloy is the most



popular titanium alloy with high strength, low density, high fracture toughness, excellent corrosion resistance and superior biocompatibility [4,5]. Its applications span a wide range of industries from medicine to aerospace. However, the low reproducibility of L-PBF and the possibility of defects in the finished products limit its application potential. Hot isostatic pressing (HIP) is a technology that allows the elimination of internal porosity in metal products through plastic deformation and diffusion [10]. The use of HIP therefore allows for increased reproducibility of L-PBF prints and, theoretically, the use of printing parameters that enable faster product construction, as it can be assumed that the porosity created during L-PBF will be removed during HIP. The aim of this article is therefore to assess the possibilities of HIP processing on Ti6Al4V products prepared with different energy densities during L-PBF and to characterize the effect of energy density on porosity and the possibilities of eliminating porosity by subsequent HIP processing.

2. MATERIALS AND METHODS

Commercially available virgin-state Ti-6Al-4V powder supplied by Renishaw was used as the feedstock material. The powder exhibited a spherical morphology with a particle size distribution of D10 = 23 μ m, D50 = 33 μ m, and D90 = 48 μ m, as determined using a Malvern MasterSizer 3000 particle size analyzer. Experimental samples were fabricated using a Renishaw AM500 laser powder bed fusion (L-PBF) system. The samples were printed in the shape of cylindrical rods with a diameter of 13 mm and a length of 130 mm. Printing was conducted in a controlled argon atmosphere, with the build platform made of titanium and preheated to 170 °C. The rods were oriented vertically during the build process. The specific printing parameters applied for each experimental series are summarized in **Table 1**. The volumetric energy density (E), which represents the average energy input per unit volume during the scanning of a single layer, was calculated using the following formula:

$$E = \frac{P}{(v \cdot h \cdot t)} \tag{1}$$

where P is the laser power, v is the scanning velocity, h is the hatch space between adjacent scan passes and t is the layer thickness. After printing, all prepared samples were subjected to heat treatment (HT) in a dynamic Ar atmosphere in a muffle furnace at a temperature of 810 °C for 2 h, including the platform, to reduce internal stress. Afterwards, they were cut from the platform using electro discharge machining (EDM) on a CHMER EDM cutter. From each series of samples, half of the samples were subsequently subjected to HIP using an EPSI hot isostatic presser. During HIP, a temperature of 800 °C and a pressure of 175 MPa were used for 2 hours. After holding at the temperature and pressure, natural cooling was used. Subsequently, transverse and longitudinal samples were taken from the bars using EDM for metallographic observations and pycnometric density measurements. Standard metallographic techniques, including grinding on SiC papers with grain sizes ranging from 60 to 2000 (grains/cm²) and polishing with Al₂O₃ suspension with particle size changing from 1 to 0.3 µm, were applied. Microstructural characterization of the samples was carried out using optical microscopy (OM) on an Olympus GX51 microscope and scanning electron microscopy (SEM) on a Quanta 450 FEG instrument equipped with an energy-dispersive X-ray spectrometer (EDS) for elemental analysis. To reveal the microstructure, the samples were etched using Kroll's reagent. The density (ρ_{pyc}) of the samples was determined via helium pycnometry using an AccuPyc II 1340 gas pycnometer with an integrated analysis module. Based on the pycnometric measurements, the closed porosity (Pc) was calculated according to the following relationship:

$$P_{cl} = \left(1 - \frac{\rho_{pyc}}{\rho_{ten}}\right) \cdot 100 \tag{2}$$

where ρ_{teo} represents theoretical density. The theoretical density of 4.51 g/cm³ were used. It is a density value that was determined experimentally by measuring the pycnometric density of the forged Ti6Al4V material. Porosity levels by image analysis method (P_{ia}) were determined by adjusting the brightness threshold, and porosity fractions were calculated automatically based on the contrast between dark porosity and bright solid



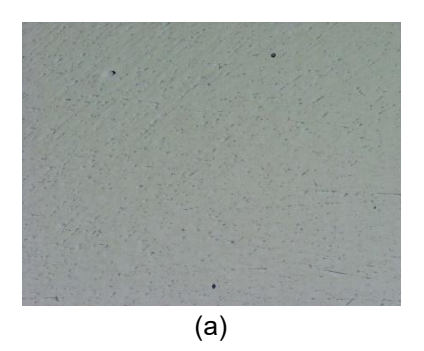
material with using imageJ software. The five different areas were analyzed with the distribution of individual analyzed areas from edge to edge of the samples in the x direction in digitalized OM images with 100x magnification. An NV XT H 225 ST tomograph was used for scanning of tomographic volumes, and 3D-CT Pro software was used for the reconstruction of the tomographic data. VGSTUDIO MAX 3.3.2 software was applied for analysis of the porosity and internal construction of scanned samples. The test samples were scanned at an accelerating voltage of 220 kV and at a power of 99 W with the size of the focal spot at about 80 µm. For the CT reconstruction, radiographic projections of 3141 volume scanned during rotation of samples by 360° were used. The time required to capture one radiographic projection took about 22 s. The tensile testing was performed on samples with a thickness of 8 mm and a length of 55 mm. The Zwick/Roell Z150 device and a strain rate of 0.5 min⁻¹ were used for testing (three measurements for each sample series).

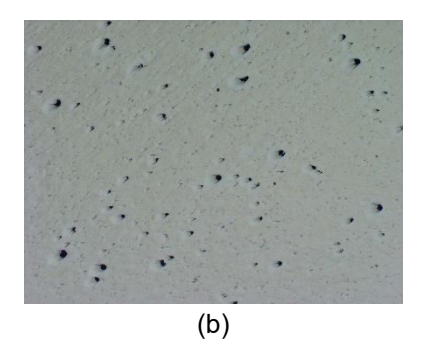
Table 1 Printing parameters used for individual series (M-meander scan strategy, CH-chessboard scan strategy)

Sample	1	2	3	4	5	6	7	8	9	10
P (W)	400	400	400	200	200	200	100	200	200	200
S (mm/s)	833	1200	1500	833	1200	1500	800	830	800	1000
Scan strategy	М	М	М	М	М	М	CH	М	CH	СН
t (µm)	60	60	60	60	60	60	30	60	30	60
h (µm)	100	100	100	100	100	100	100	100	100	100
E (J/mm³)	80	55.6	44.4	40	27.8	22.2	41.7	40.2	83.3	33.3
Print time (h)	22	17	14	22	17	14	61	23	61	19

3. RESULTS AND DISCUSSION

A range of energy densities from 22 to 83 J/mm³ was applied across the sample series (as previously listed in **Table 1**), which resulted in variations in porosity levels. Selected OM images of polished metallographic sections in the as-printed condition, subjected only to stress-relief heat treatment, are presented in **Figure 1**.





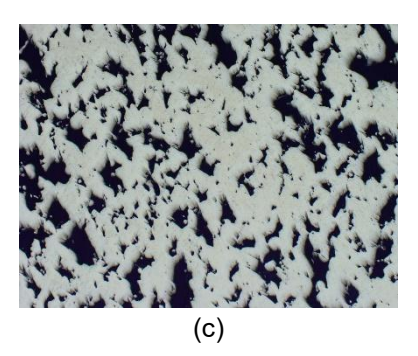


Figure 1 Optical microscopy (OM) images of metallographic cross-sections of selected sample series in the as-printed condition: (a) series 1, (b) series 4, (c) series 6. All images were captured at the same magnification and correspond to transverse sections

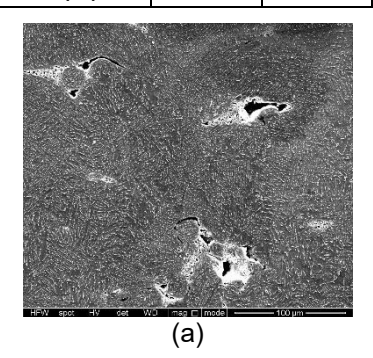
The porosity values, as determined by pycnometric measurements and image analysis, for each sample series are presented in **Table 2**. When high energy densities (approximately 80 J/mm^3) were used, predominantly spherical pores with diameters up to 40 µm were observed. In contrast, medium energy densities (around 40 J/mm^3) resulted in a mixture of larger spherical pores and irregularly shaped pores up to 100 µm in size (see **Figure 2a,b**). However, even at high energy densities, the presence of irregular pores was occasionally detected, which can be attributed to local imperfections in the powder bed (see **Figure 2c**). Low energy densities ($20-30 \text{ J/mm}^3$) led to the formation of a high volume fraction of irregular porosity, with some pores reaching sizes up to 500 µm, primarily due to insufficient energy input, which results in inadequate interlayer bonding. As shown in the aforementioned **Table 2**, it is evident that the application of higher laser powers can mitigate the influence of increased scanning speeds on porosity content, this is particularly clear when

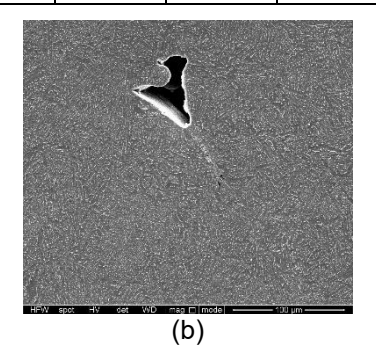


comparing series 2 and 5 with series 3 and 6 (prior to HIP treatment). **Table 2** also includes the porosity values after hot isostatic pressing (HIP). The results demonstrate that HIP significantly reduced porosity across all series. In samples produced with high and medium energy densities (40–80 J/mm³), HIP eliminated internal porosity, reducing it to values close to zero. For samples processed with low energy densities (20–30 J/mm³), HIP also led to a notable reduction in porosity, although the final content remained at approximately 1–2 %. The limited HIP efficiency in these cases is attributed to the large pore sizes and interconnected porosity, which restrict plastic deformation during consolidation. A similar trend has been reported for L-PBF-fabricated 316L steels, as noted in [10]. In general, it can be concluded that the applied HIP conditions become increasingly ineffective in eliminating porosity for samples produced with energy densities below 35 J/mm³. **Figure 3a and 3c** presents tomographic cross-sections of samples from series 8 and 10, respectively in the as-printed state. As can be seen in the aforementioned images, various printing parameters led to different porosity contents and, in particular, higher scan speed led to high pore content, in accordance with the results in **Table 2**. **Figure 3b** and **3d** shows the same sample series after HIP treatment. As shown, in the mentioned figures, porosity was completely eliminated by HIP in series 8. In contrast, series 10 exhibited only a partial reduction, with residual pores up to 200 µm remaining after treatment.

Table 2 Porosity content values determined by helium pycnometer and optical image analysis for individual sample series, before and after hot isostatic pressing (HIP) treatment

Before HIP										
Sample	1	2	3	4	5	6	7	8	9	10
$ ho_{pyc}$ (g/cm 3)	4.500	4.444	4.380	4.430	4.459	4.206	4.469	4.498	4.499	4.412
Pcl (%)	0.20	1.45	2.89	1.78	1.13	6.75	0.91	0.26	0.24	2.18
P _{ia} (%)	0.11	1.22	2.88	0.91	1.68	5.00	1.06	0.03	0.08	2.60
After HIP										
Sample	1	2	3	4	5	6	7	8	9	10
$ ho_{pyc}$ (g/cm 3)	4.508	4.504	4.505	4.508	4.469	4.433	4.449	4.505	4.506	4.475
Pcl (%)	0.03	0.14	0.10	0.05	0.91	1.71	0.24	0.10	0.09	0.77
P _{ia} (%)	0.01	0.02	0.01	0.01	0.98	1.36	0.05	0.01	0.01	0.35





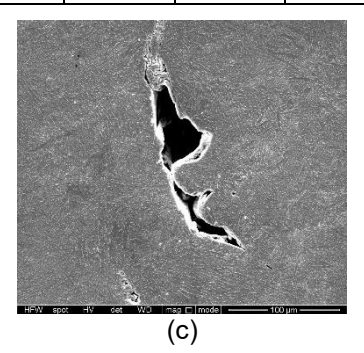


Figure 2 SEM images of metallographic sections of series in the as-printed state: (a) series 7, (b) series 8, (c) series 9; (etched, transverse section)

Figure 4 shows examples of the microstructure of selected sample series before and after HIP treatment. As can be seen in **Figures 4a**, **b**, HIP treatment did not significantly affect the microstructure and even after HIP it shows a typical fine cellular microstructure typical of L-PBF preparation [4,5]. The fine network, which is shown in the images in a brighter shade than the dark matrix, consists of a V-enriched β phase [4,5]. Apart from various porosity contents, different printing parameters and HIP processing under the stated conditions had no significant effect on the microstructure and consist of α laths and smaller amount of beta phase (see **Figure 4c**).

Table 3 characterizes the tensile mechanical properties for several selected sample series before and after application of HIP treatment. As can be seen, different printing parameters significantly affect the mechanical



properties and the use of low energy densities, and the associated porosity causes low strengths and almost zero ductility. The application of HIP processing significantly increases the ductility of almost all the above series of samples, apart from samples for which HIP was not effective due to the high number of interconnected pores. It can also be seen from the above properties that HIP processing does not significantly affect the yield strength, and the yield strength decreases only by values lower than 40 MPa. **Table 3** also shows the mechanical properties of commercially available Ti6Al4V alloy Grade 5 ELI ASTM F136, tested under the same conditions. As can be discerned, samples from series 1, 9 both in the as-printed state and after HIP and series 10 after HIP show higher yield strength and ultimate strength than the commercially available alloy, however, the ductility is better for the commercially available alloy. For samples from series 5 and series 10 in the printed state, very low strengths were found, and the yield strength could not be determined due to minimal ductility, caused by the relatively high porosity content.

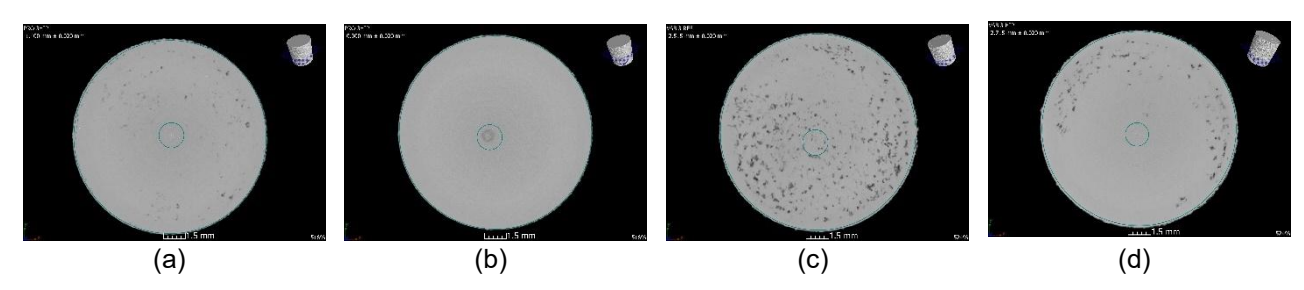


Figure 3 X-ray computed tomography sections of selected sample series: (a) series 8 in the as-printed state, (b) series 8 after HIP treatment, (c) series 10 in the as-printed state, (d) series 10 after HIP treatment

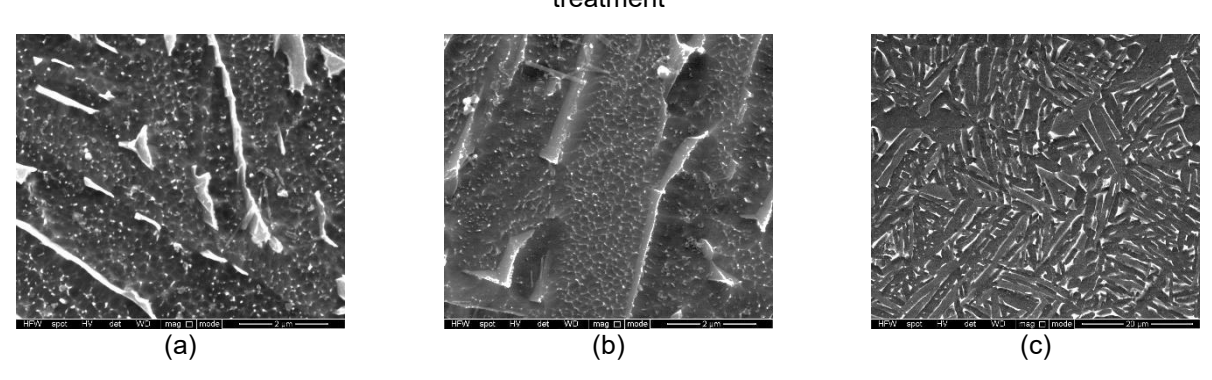


Figure 4 SEM images of metallographic sections of sample series 10: (a) as-printed state, transverse section; (b) after HIP treatment, transverse section; (c) after HIP treatment, longitudinal section. All microstructure images are etched state

Table 3 Resulting mechanical property values of tensile testing

Series	State	<i>E</i> (GPa)	R _{0,2} (MPa)	R _m (MPa)	A (%)				
5	As-printed	96.8 ± 7.7	-	477 ± 41	0.4 ± 0.3				
	HIP	111.9 ± 3.5	-	661 ± 23	0.6 ± 0.2				
1	As-printed	115.6 ± 4.4	1022 ± 9	1088 ± 6	10.3 ± 2.0				
	HIP	116.0 ± 5.1	999 ± 12	1069 ± 6	12.9 ± 0.9				
9	As-printed	111.0 ± 3.8	973 ± 12	1074 ± 38	4.5 ± 3.5				
	HIP	112.4 ± 2.7	947 ± 4	1085 ± 3	9.7 ± 1.3				
10	As-printed	107.4 ± 3.4	-	831 ± 175	1.0 ± 0.4				
	HIP	113.8 ± 3.0	990 ± 10,3	1093 ± 10	7.7 ± 0.4				
Cast	Forged	108.4 ± 3.1	911 ± 13	945 ± 8	16.1 ± 0.8				



4. CONCLUSION

Ti-6Al-4V alloy samples were fabricated via laser powder bed fusion (L-PBF) using a range of processing parameters. The applied printing conditions had a pronounced influence on the resulting porosity characteristics, with porosity contents ranging from 0.2 % to 6.8 %. Higher porosity levels were observed in samples produced using lower energy densities, indicating insufficient energy input for complete layer bonding. Hot isostatic pressing (HIP) significantly reduced porosity in most cases, bringing values below 0.3 %, except for samples processed with energy densities below 35 J/mm³. In these cases, the presence of large, interconnected pores limited the effectiveness of the HIP treatment due to constrained plastic deformation during consolidation. The tensile mechanical properties of the alloy were also strongly influenced by the applied energy density and the associated porosity content. Post-HIP treatment led to notable improvements in ductility, primarily due to the elimination of internal porosity. Importantly, the selected HIP parameters preserved the fine cellular microstructure characteristic of L-PBF-processed Ti-6Al-4V alloy. As a result, samples produced with medium to high energy densities retained high yield strength values exceeding 950 MPa, demonstrating the potential for achieving a favourable balance between strength and ductility through optimized processing and post-processing conditions.

ACKNOWLEDGEMENTS

This work was supported by the project TN02000018 "National Centre of Competence for Engineering" and by the project SP2025/080 "Development and implementation of a measuring device for sound absorption measurement of materials at low excitation frequencies".

REFERENCES

- [1] OLIVEIRA, J.P., LALONDE, A.D., MA, J. Processing parameters in laser powder bed fusion metal additive manufacturing. *Materials and design*. 2020, vol.193, 108762. https://doi.org/10.1016/j.matdes.2020.108762.
- [2] HUANG, R., RIDDLE, M., GRAZIANO, D., WARREN, J., DAS, S., NIMBALKAR, S., CRESKO, J., MASANET, E. Energy and emissions saving potencial of additive manufacturing: The case of lightweight aircraft components. *Journal of cleaner production.* 2016, vol. 135, pp. 1559-1570. https://doi.org/10.1016/j.jclepro.2015.04.109.
- [3] ALLEN, J. An investigation into the comparative costs of additive manufacture vs. machine from solid for aero engine parts. *Cost Effective Manufacture via Net-Shape Processing*, 2006, vol. 17, pp. 1-17.
- [4] LIU, S., SHIN, I.C. Additive manufacturing of Ti6Al4V alloy: A review. *Materials and design*, 2019, vol. 164, 107552. https://doi.org/10.1016/j.matdes.2018.107552.
- [5] GHIO E, CERRI, E. Additive manufacturing of AlSi10Mg and Ti6Al4V lightweight alloys via laser powder bed fusion: A review of heat treatments effects. *Materials*. 2022, vol. 15, no. 6, p. 2047. https://doi.org/10.3390/ma15062047.
- [6] MATHEWS, M.J., GUSS, G., KHAIRALLAH, S.A., RUBENCHIK, A.M., DEPOND, P.J., KING, W.E. Denudation of metal powder layers in laser powder bed fusion processes. *Acta Materialia*. 2016, vol. 114, pp. 33-42, ISSN 1359-6454, https://doi.org/10.1016/j.actamat.2016.05.017.
- [7] GELATKO, M., HATALA, M., BOTKO, F., VANDŽURA, R., HAJNYŠ, J., ŠAJGALIK, M., TOROK, J. Stress relieving heat treatment of 316L stainless steel made by additive manufacturing process. *Materials*. 2023, vol. 16, no. 19, p. 6461. https://doi.org/10.3390/ma16196461.
- [8] MA, Q.-P., MESICEK, J., FOJTIK, F., HAJNYS, J., KRPEC, P., PAGAC, M., PETRU, J. Residual stress build-up in aluminum parts fabricated with SLM technology using the Bridge curvature method. *Materials*. 2022, vol. 15, no. 17, p. 6057. https://doi.org/10.3390/ma15176057.
- [9] HITZLER, L., HIRSCH, J., HEINE, B., MERKEL, M., HALL, W., ÖCHSNER, A. On the anisotropic mechanical properties of selective laser-melted stainless steel. *Materials*. 2017, vol. 10, no. 10, p. 1136. https://doi.org/10.3390/ma10101136.
- [10] CEGAN, T., PAGAC, M., JURICA, J., SKOTNICOVA, K., HAJNYS, J., HORSAK, L., SOUCEK, K., KRPEC, P. Effect of hot isostatic pressing on porosity and mechanical properties of 316L stainless steel prepared by the selective laser melting method. *Materials*. 2020, vol. 13, no. 19, p. 4377. https://doi.org/10.3390/ma13194377.